Manganese oxide biomineralization is a social trait protecting against nitrite toxicity.

Christian Zerfaß[a,b], Joseph A. Christie-Oleza[a,b], and Orkun S. Soyer[a,b,*]

[a] School of Life Sciences, BBSRC/EPSRC Warwick Integrative Synthetic Biology Centre (WISB), University of Warwick, Coventry, CV4 7AL, UK. [b] Warwick Integrative Synthetic Biology Centre (WISB), University of Warwick, Coventry, CV4 7AL, UK.

KEYWORDS: microbial ecology, biomineralization, metal recovery, biotechnology, community function, social behavior, exoenzyme, reactive oxygen species, *Roseoabacter sp.* AzwK-3b.

Corresponding Author

* O.Soyer@warwick.ac.uk (O.S.S.)

Abstract

Manganese bio-mineralization by oxidation is a costly but, still, widespread process among bacteria and fungi. While certain potential advantages of manganese oxidation have been suggested, to date there is no conclusive experimental evidence for, how and if this process impacts microbial fitness in the environment. Here we show how a model organism for manganese oxidation, *Roseobacter sp.* AzwK-3b, is growth-inhibited by nitrite, and that this inhibition is mitigated when manganese is added to the culture medium. We show that manganese-mediated mitigation of nitrite-inhibition is dependent on the culture inoculum size, with larger inocula being able to withstand higher concentrations of nitrite stress. Furthermore, the bio-mineralized manganese oxide (MnO_X) forms granular precipitates in the culture, rather than sheaths around individual cells. These findings support the notion that MnO_X is a shared community product that improves the cultures' survival against nitrite-stress. We show that the mechanistic basis of the MnO_X effect involves both its ability to catalyze nitrite oxidation into (non-toxic) nitrate under physiological conditions, and its potential role in influencing redox chemistry around reactive oxygen species (ROS). Taken together, these results provide for the first direct evidence of improved microbial fitness by MnO_X deposition in an ecological setting, i.e. mitigation of nitrite toxicity, and point to a key role of MnO_X in handling stresses arising from ROS. These findings could be of general relevance for all organisms oxidizing manganese, allowing them to offset costs associated with extracellular bio-mineralization.

Introduction

A large variety of biominerals based on different cations (e.g. iron, manganese, calcium) and anions (e.g. carbonates, oxides, phosphates) are deposited by different microorganisms (1). One of these is manganese oxide (2–5), which is deposited by the oxidation of soluble Mn^{II}. Microbial Mn^{II} oxidation received attention with the discovery of polymetallic, manganese-rich biogenic deep sea nodules, which have been shown to harbor both manganese-oxidizing, and manganese-reducing organisms (6). While it is suggested that such nodules could potentially be mined for rare earth elements, and that the associated metal-active organisms utilized in biotechnology of metal recovery (2, 3, 5–8), it remains unclear in many cases why organisms show such metal-oxidizing and -reducing activities. In

the case of metal-reducing organisms, it has been shown that metabolic energy can be gained under anaerobic conditions from using metal oxides (i.e. manganese, iron, or others) as an alternative terminal electron acceptor (9–11). The potential evolutionary advantages of metal-oxidation, and in particular manganese oxidation meanwhile is not well understood (2, 7, 8).

Some metals can be oxidized by microbes and act as an inorganic energy source for so-called chemolithotrophic growth, as in the case of iron lithotrophy (12). Chemolithotrophy on manganese has been suggested but little experimental evidence has been found so far (2). Two other common hypotheses for manganese oxidation are that the resulting manganese oxides (MnO_X) can icrease accessibility of organic nutrients or protect microbes from potentially toxic compounds (13). The validity of the latter hypothesis remains to be tested conclusively. MnO_X has been shown to react with complex organic (i.e. humic) substances (14), but it is not clear if the resulting organic products form such reactions are utilized by microbes. It is suggested that certain fungi employ ligand-stabilized Mn^{III} to oxidize recalcitrant litter (15), but these studies were not performed with single (defined) carbon/energy sources. Similarly, the former hypothesis regarding the protective potential of MnO_X remains unproven to date (2, 7). It has been suggested that MnO_X precipitates can act as strong sorbents of heavy metals, hence mitigating the toxic effects of such metals on microorganisms, but this has yet to be tested in a biological context (2). Taken together, the biological significance of microbial manganese oxidation remains a paradox, as no benefits have been demonstrated for this costly metabolic process

In recent years, *Roseobacter sp.* AzwK-3b emerged as a model organism to study the generation of MnO_X (16). AzwK-3b is a bacterium that shows significant manganese oxidizing activity *in vitro* when grown in a complex (rich) K-Medium (16). This activity was shown to be mediated by a secreted exoenzyme - a haem type oxidase - that can catalyze the generation of superoxides from NADH and oxygen. The resulting superoxide can in turn facilitate the Mn^{II} oxidation into Mn^{III}, which undergoes further disproportionation to result in MnO_2 (17–21) – or more specifically mixed valence state MnO_X. The required NADH for this exoenzyme-mediated reaction is presumably secreted also by AzwK-3b (17). Thus, these mechanistic findings strongly suggest that AzwK-3b is making a significant metabolic investment into

production of MnO_X. It is currently not clear how such a costly strategy benefits individual cells and how it could have been maintained over evolutionary timescales.

In an attempt to better understand the 'fitness' impact of manganese oxidation, we have studied the physiology of *Roseobacter sp.* AzwK-3b in more detail. We identified a defined medium composition that allowed growth of this bacterium both with and without manganese. While we found no significant differences in growth rate under these two conditions, we found that the manganese oxidizing activity of *Roseobacter sp.* AzwK-3b supports growth of the bacterium at nitrite concentrations that fully prevent growth in a manganese-free culture. We found that MnO_X forms as granules dispersed among cells, and its nitrite-inhibition mitigation effects show a significant population size effect, conforming to a 'community commodity' nature of this compound. Mechanistically, we show that biogenic MnO_X was able to catalyze nitrite oxidation into nitrate under physiological conditions, and that the mitigation of nitrite-inhibition was also affected by NADH. These results suggest that the ability of MnOx to alleviate nitrite toxicity relates to providing catalytic scavenging of reactive oxygen species (ROS) within the environment.

Results

To study the role of manganese oxidation on microbial fitness we have focused here on *Roseobacter sp.* AzwK-3b, which has recently emerged as a model organism for this process (2, 8). We refer to the oxidation product as MnO_X, since biogenic manganese oxides are usually precipitates with mixed manganese oxidation states, particularly Mn^{II}, Mn^{III} and Mn^{IV} (2, 26). AzwK-3b has been shown to oxidize manganese to MnO_X by means of an excreted exoenzyme and NADH, and potentially involving an elaborate redox reaction path (17–21). We have first attempted to identify fully-defined growth conditions for this bacterium, which has been to date studied in complex K-medium (16), an artificial seawater derived, peptone/yeast extract containing medium (16, 27). Through systematic analysis of media composition, we have created a fully defined medium that supports AzwK-3b growth (from now on referred to as modified artificial seawater medium, ASW_m) (Table 1). This exercise revealed also the requirement for five vitamin supplements for growth (Figure S1). Given this defined culture medium, we were then able to interrogate the impact of manganese on the growth of AzwK-3b.

Manganese oxidation does not impact growth rate. Despite potentially significant costs associated with exoenzyme and NADH investment, we did not find any substantial difference in growth rates and steady state population sizes with increasing Mn^{II} concentration and with 25 mM acetate (Figure 1). A slightly slower growth at the highest manganese concentration (500 μM) was observed, but it was difficult to ascertain this effect, as both MnO_X particles and cells co-aggregating with those particles could have interfered with the absorbance measurements. The slightly reduced growth rate at 200 μM $Mn^{II}Cl_2$ is in line with an earlier report on AzwK-3b, where 100 μM Mn^{II} was found to decrease the growth rate in (complex) K-medium (16). Other manganese-oxidizing bacteria, such as *Erythrobacter sp.* SD-21 (28, 29) and a marine *Bacillus* strain (30), were reported to grow better when cultured with Mn^{II}-supplement. In light of these different findings and possible difficulties with growth rate measurements in the presence of manganese precipitation, we cannot be fully conclusive about the growth effects associated with manganese oxidation based on the presented results, however, they are suggestive of a low or no-impact on growth rate.

Manganese oxidation mitigates nitrite growth inhibition. With growth effects being limited, a possible alternative explanation for a positive role of manganese oxidation is a protective effect against inhibitors or stresses (2, 13). Here, we evaluated this hypothesis for nitrite. Nitrite is commonly found in the environment, where it results from the reduction of nitrate, a key terminal electron acceptor utilized by many microbes (31). We found nitrite inhibited the growth of AzwK-3b in manganese-free cultures, where already as little as 0.25 mM nitrite prevented growth of AzwK-3b (Figure 2A). No growth was detected at and above 0.5 mM nitrite. Note that a salinity effect at such low concentrations of nitrite (which was added as sodium nitrite) is highly unlikely. To further rule out this possibility, we additionally analyzed the growth of AzwK-3b at different salinity levels using concentrations of sodium chloride from 200 mM (default in the defined ASW_m medium employed here) up to 428 mM (default in the ASW medium (22)). This confirmed that salinity effects on growth in this range are minimal (Figure S2), and higher salinity is rather favorable for AzwK-3b growth. Thus, the effects of nitrite are due to toxicity rather than salinity.

With the addition of 200 μM Mn^{II}, we found that AzwK-3b is able to grow in the presence of up to 1 mM nitrite (Figure 2B). Increasing the nitrite concentration still affected both the growth rate and maximal culture density (based on A_{600}), but this effect was much lower compared to the manganese-free cultures (Figure 2). To overcome any potential confounding effects of MnO_X precipitation on spectroscopic culture density measurements, we additionally quantified acetate consumption by ion chromatography as a proxy for growth. As expected, manganese-free cultures with 0.25 mM (or higher) nitrite showed only insignificant decrease in acetate, while the Mn^{II} supplemented cultures showed acetate consumption in accordance with the A_{600} measurements (see Figure S3). These findings confirm that Mn^{II} supplementation allows AzwK-3b to withstand nitrite inhibition.

Nitrite-inhibition relief is a community function that depends on culture size and that is mediated by dispersed, granular MnO_x precipitates. It has been shown that MnO_X precipitation by AzwK-3b is mediated by secreted exoenzymes (17). It is not known, however, whether the process of MnO_X precipitation occurs primarily on individual cell surfaces, or whether it is a population level process with the secreted enzymes conferring to the notion of a "community commodity" (32–35). We hypothesized that these two different scenarios could be distinguished by analyzing population size effects on MnO_X mediated mitigation of nitrite-inhibition. In particular, we designed an experiment in which cultures pre-grown without Mn^{II} are subsequently sub-cultured into media with Mn^{II} and nitrite, using different inoculum size (Figure S4). We argue that in the case of MnO_X precipitation being a process confined to individual cells, there should be no effect of inoculation size.

We found that manganese mediated mitigation of nitrite inhibition was dependent on inoculum size (Figure 3). A pre-culture was grown without nitrite and manganese, and from this, inocula were generated at two different time points within the first third of the exponential phase (labelled IT1 and IT2 in Figure S4). When these inocula were subjected to nitrite in the main-culture, the earlier, low-density inoculum IT1 was inhibited by nitrite regardless of the presence or absence of Mn^{II} (Figure 3 A,B), while manganese-mediated mitigation of nitrite inhibition was clearly evident for the larger, high-density inoculum IT2 (Figure 3 C,D). In the IT1 cultures half of the acetate was unused at 0.25 mM nitrite, and gradually more acetate resided with increasing nitrite concentration (Figure S5). In the IT2

cultures with Mn^{II} supplementation, however, acetate was completely removed at all nitrite levels below 2.5 mM and only 25 – 50 % of acetate remained at 5 – 10 mM nitrite. In the control samples (no inoculation) there was no change in acetate concentration ruling out any cross-activity with manganese.

Rather than a true population size effect, these observed inocula effects could be due to cells from the Mn-free, early-phase pre-cultures not having 'turned on' expression of exoenzymes required for MnO_X precipitation. To rule out this possibility, we performed an additional experiment, where the pre-cultures were already grown with 200 μM Mn^{II}. Using this pre-adapted culture, inocula were again prepared by sampling at different growth time points (IT 1 – 4 in Figure S6, A). Cultures grown from these different inocula displayed much weaker inhibition by increasing nitrite concentrations up to 10 mM (Figure S6, B) and were able to consume acetate (Figure S6, C), yet there were still inoculum size effects on overcoming nitrite inhibition (Figure 4, green). Interestingly, the extent of this effect seems similar to that observed with inocula originating from pre-cultures grown without Mn^{II} but supplied with Mn^{II} after subculturing into nitrite containing media (Figure 4, blue). In particular, at 5 and 10 mM nitrite, maximum growth rate (and final density) data from all these cultures showed a strong nonlinear correlation to initial inocula density that can be fitted to a sigmoidal curve. (Figure 4, black line). The infliction point of this curve happened at a lower inoculum size for those cultures that were not supplied with Mn^{II} at any stage (Figure 4, red). Thus, we conclude that there is an inoculum density effect on the ability of Mn^{II} supplemented cultures to tolerate nitrite irrespective of their culturing history, but that this effect is stronger for cultures not pre-grown with Mn^{II}. There were no such effects without nitrite or without Mn^{II} (Figure 4).

These results strongly suggest that MnO_X precipitation is a community level function. To further collaborate on this result, we explored the micro-structure of the AzwK-3b cultures in the presence of Mn^{II}. Analysis of cultures using electron microscopy revealed that MnO_X precipitates as granules dispersed within the culture, and attaching to clusters of cells, rather than forming sheaths around individual cells (as seen in some other cases of metal oxide precipitations (36)) (Figure 5, left). Employing electron dispersive X-ray spectroscopy, we confirmed that these granular structures contained manganese, while no manganese was detected in locations with cells only (i.e. without granular structures, see Figure 5, right).

MnO_X mediated nitrite protection involves redox reactions and oxygen radicals. After establishing the community level functionality of biogenic MnO_X as a protective agent against nitrite, we next wanted to evaluate the mechanistic basis of this function in the context of nitrite toxicity. While multiple mechanisms of nitrite-toxicity are reported (37, 38), two key reactive species are usually implicated, i.e. free nitrous acid (39) and peroxynitrite. The former forms through protanation of nitrite, while the latter forms from the reaction of nitrite with hydrogen peroxide (40–42). Thus, two non-exclusive, possible mechanisms of MnO_X relief on nitrite toxicity are: (i) MnO_X catalyzed oxidation of nitrite to nitrate (a reaction that has been shown to be feasible chemically under low pH (43)) and thereby avoiding formation of either free nitrous acid or peroxynitrite; or (ii) MnO_X catalyzed degradation of hydrogen peroxide and thereby avoiding the reaction of this compound with nitrite to form peroxynitrite.

To see if AzwK-3b generated MnO_X can catalyze nitrite oxidation under physiological conditions, we collected it from culture supernatants and evaluated its reactivity with nitrite in our ASW_m-medium at pH = 8.0. Over 27 days, we found nitrite oxidation by biogenic MnO_X in a dose dependent manner, while neither synthetic MnO_2 powder nor the MnO_X-free supernatant solution showed any significant nitrite oxidation (Figure 6A). The trend of nitrite oxidation matched with nitrate production (Figure 6B), thus confirming the assumed reaction pathway of nitrite-oxidation into nitrate (43). Taking into account the difficulties of accurately determining the amount of precipitated MnO_X that were added into the nitrite assay, we can still estimate that the condition with highest MnO_X levels contained at least 1-2 mM (with respect to Mn). This presents a stoichiometric minimum 2-fold excess over nitrite (at 0.5 mM), hence enough for complete nitrite oxidation. The fact that this reaction didn't proceed further than an oxidation of ~0.18 mM nitrite (i.e. ~35 %) indicates that either the biogenic MnO_X was only partially reactive or that its reactivity reduced over time (as known to be the case for synthetic manganese oxides (2, 13)). Sample pH remained relatively stable with the biogenic MnO_X, while samples without manganese and with synthetic MnO_2 reached a pH of 6.9 and 6.8, respectively at the end of the experiment (from an initial pH of 8.2 of the medium). This acidification of the control samples might be due to carbon dioxide dissolution, which might have been buffered in the samples with biogenic MnO_X due to proton consumption during

nitrite oxidation, or due to co-precipitated organic solutes (polymers, proteins) from the cell-free supernatant.

These findings confirmed that the biogenic MnO_X were capable to oxidize nitrite at physiological conditions, and prompted us to test MnO_X mediated nitrite oxidation directly in AzwK-3b cultures. We found some evidence for decreasing nitrite concentration in different cultures tested, but this was not significant (Figure S7), and some decrease was also seen in the manganese free cultures (indicating possible measurement effects in the solution). If nitrite oxidation was the main mechanism of MnO_X mediated protection *in vivo*, these cultures would have been expected to oxidize most of the nitrite present in the media. Thus, we conclude that under our experiment conditions nitrite-oxidation was only a potential contributing factor.

A plausible alternative mechanism of MnO_x mediated nitrite-inhibition relief could be related to formation of reactive peroxynitrite, which is shown to be highly toxic to bacteria (41, 42, 44, 45), and which can form at low pH from the reaction of hydrogen peroxide with nitrite (40). If peroxynitrite is the main species underpinning nitrite toxicity, then, MnO_X protection against nitrite could be due to its ability to degrade hydrogen peroxide and thereby reducing the rate of peroxynitrite formation. The reactivity of MnO_X towards hydrogen peroxide has been demonstrated chemically (40, 46–53), but never shown or tested in a biological context. Here, we hypothesized that if these types of redox reactions were involved in MnO_X mediated mitigation of nitrite-inhibition, the process dynamics can be modulated with the introduction of additional hydrogen peroxide or NADH (which can help increase the rate of MnO_X formation (18), but which can also be directly involved in hydrogen peroxide reduction through peroxidase-catalysed reactions (54–58)). To test this hypothesis, we again grew pre-cultures of AzwK-3b without Mn^{II} and sub-cultured these in medium containing Mn^{II} and nitrite, but at the same time also spiking in hydrogen peroxide or NADH. Hydrogen peroxide spiking did not show any effect on nitrite inhibition or its release by Mn^{II} supplementation (Figure S8), possibly due to spiked hydrogen peroxide being cleared primarily through additional peroxidases rather than impacting MnO_x mediated process dynamics. In line with this hypothesis, spiking NADH resulted in full mitigation of nitrite inhibitory effect (even without Mn^{II}) (Figure 7). This suggests that nitrite toxicity relates to peroxynitrite formation via hydrogen peroxide, which can be decomposed by MnO_X (as

shown before (40, 46–53)) or NADH-utilizing peroxidases (that are shown to be present in Roseobacter species including AzwK-3b (17, 59) (see also Table S1)).

Discussion

Manganese bio-mineralization into MnO_X is widespread among bacteria, but there is no clarity about its evolutionary advantage. Here, we developed a defined growth media for the manganese oxidizing model organism *Roseobacter sp.* AzwK-3b and demonstrated that this organism's strong growth-inhibition by nitrite is mitigated through its ability to precipitate biogenic MnO_X. We found that this MnO_X-mediated mitigation of nitrite toxicity is dependent on population size, and that MnO_X forms dispersed granules that are attached to clusters of cells in the population. These observations, combined with the established role of exoenzymes in the formation of MnO_X precipitates, suggests that these provide a community function to AzwK-3b and allows cultures grown to sufficient density in the presence of manganese to become resistant to the inhibitory effects of nitrite. Our attempts to elucidate the mechanistic basis of this functionality showed that biogenic MnO_X can oxidise nitrite to nitrate (under conditions that synthetic MnO_2 cannot). Together with the known ability of MnO_X to degrade hydrogen peroxide (40, 46–53), these findings show that biogenic MnO_X can inhibit the two key routes to the formation of reactive nitrite species.

These findings provide for the first-time a direct evidence for the impact of MnO_X on an organism's growth, thus demonstrating a positive fitness effect and a possible evolutionary explanation to the costly process of MnO_X oxidation. Other suggested functional roles for this process to date were either hypothetical or were based on experiments with synthetic manganese oxide counterparts (2, 7, 8), and none of them were fully confirmed in a biological context. While mitigation of nitrite inhibition might not be the only evolutionary advantage of MnO_X oxidation in AzwK-3b or other manganese oxidizing species, it is definitely an ecologically relevant function. Nitrite is a known inhibitor in the environment (37, 38, 60), including in wastewater treatment applications (39). In the case of AzwK-3b, this ecological relevance is highly suggestive, as this species was isolated from an "agriculturally impacted, shallow salt marsh" (16) where nitrite (among other nitrogen species) can occur due to microbial conversion of nitrogen fertilizers (61–64). It is also interesting to note that oceanic manganese-rich modules are found to contain both manganese oxidizing and reducing

286 bacteria (6), with current-day representatives of the latter group, such as *Shewenalla*
287 *oneidensis* (9), also being nitrate-reducers (65–67).

288 Our study opens up additional investigations into the mechanism of nitrite toxicity and
289 the role of MnO_X oxidation in it. Multiple mechanisms of nitrite-inhibition of bacteria have
290 been reported (37, 38), and a key role for free nitrous acid (i.e. protonated nitrite) (39) and
291 peroxynitrite, from nitrite and hydrogen peroxide (40–42), is proposed. Both molecules can
292 prevent chemiosmotic coupling, and are primarily formed at low pH (nitrite is often found to
293 inhibit bacteria growth at pH < 7 (41, 42)). The formation of these reactive nitrite species can
294 be enhanced in the vicinity of the cells, where a locally lowered pH (from chemiosmotic
295 coupling) and an increased hydrogen peroxide concentration (due to cellular metabolic
296 activity (44, 45, 54, 58, 68–75)) can be formed. Interestingly, these very local conditions could
297 be avoided through the presence of MnO_X, which can degrade hydrogen peroxide and
298 catalyse the oxidation of nitrite to nitrate, which is a proton consuming process with increased
299 rate at low pH (43). The latter proposition is confirmed here for the first time, as we show
300 that biogenic MnO_X can catalyze nitrite oxidation even under physiological conditions (i.e. pH
301 8).

302 The former hypothesis, i.e. that MnO_x can interfere with nitrite toxicity operating
303 through peroxynitrite formation with hydrogen peroxide remains to be fully confirmed. Our
304 experiments with spikes of hydrogen peroxide did not alter the gross dynamics of MnO_X
305 mediated nitrite-inhibition relief, but this could be due to the design of these experiments
306 with hydrogen peroxide delivered in single doses rather than being delivered in a controlled
307 manner in the vicinity of the cells. A single dose could have been readily dealt with additional
308 peroxidases, without altering MnO_X mediated effects. On the other hand, our observation
309 that the nitrite-stress is fully mitigated in NADH-supplemented cultures (even in the absence
310 of MnO_X) lends support to the idea that nitrite stress is mediated primarily through formation
311 of peroxynitrite. In that case, the reductive power of NADH could be employed by
312 peroxidases, as well as MnO_X, to reduce hydrogen peroxide (54–56) and thereby stopping
313 the formation of peroxynitrite, explaining the observed mitigation effect of NADH.

314 These possible mechanistic scenarios of nitrite toxicity and roles of NADH,
315 peroxidases, and MnO_X in mitigating it, raise the question about why cells that already have
316 several peroxidases, such as AzwK-3b (17, 59) (see also Table S1), might invest additional

317 energy in the formation of MnO_X precipitates. The answer might relate to the exact reaction
318 mechanisms of ROS scavenging. It has been suggested, for example, that different ROS
319 scavenging enzymes have different substrate affinities and efficiencies (58). In this context
320 MnO_X – mediated scavenging could be preferred under certain ROS concentrations and
321 modes of production. In addition, and unlike peroxidases that require stoichiometric
322 equivalents of reductans as e.g. NADH/NADPH for hydrogen peroxide reduction (57, 58),
323 MnO_x at its different oxidation states (II, III, IV) can directly catalyze degradation of hydrogen
324 peroxide without NADH involvement (18, 19, 21, 40, 46–53). The fact that some peroxidases,
325 as well as the AzwK-3b enzyme catalyzing MnO_X formation, are exoenzymes (17, 76) could be
326 also highly relevant. The expression of such exoenzymes is a 'social trait', that can be
327 exploited by cheating cells that do not invest the costs but reap the benefits (32–35). The
328 presented finding that MnO_X forms dispersed granules in the culture shows that, in this case,
329 the functional effects of the exoenzyme is localized. This kind of localization is a known
330 strategy to stabilize a social trait in the face of evolution of cheating, as seen in exoenzymes
331 with localized actions, involved in sugar degradation (77) and metal scavenging (78). Thus,
332 the NADH investment into the formation of MnO_x mediated protection might be a
333 metabolically less costly strategy that is also socially more stable.

334 Within a wider context, our findings could be highly relevant to understand the
335 different forms of metal mineralization observed in different microorganisms and under
336 different ecological contexts. Given the abundance of microorganisms being involved in
337 reactions of the nitrogen cycle, there is indeed potential transient accumulation of nitrite in
338 different environments. It is also possible that MnO_X (or other minerals) can provide more
339 broad protection against ROS chemistry. For example, manganese oxidation is also observed
340 in spore-forming bacteria (79, 80), fungi and other microorganisms (as reviewed and shown
341 in (2, 36)), where a role for nitrite stress remains to be elucidated. Our findings will facilitate
342 such further studies of bio-mineralizing organisms and their different functional motives and
343 social strategies.

344 ## Materials and Methods

345 **Bacterial Strain and Culture Conditions.** *Roseobacter sp.* AzwK-3b was obtained from Colleen
346 Hansel (Woods Hole Oceanographic Institution, Falmouth, MA/USA), who isolated the strain

(16). Cultures were grown in a defined medium, which was established by modifying the pre-defined artificial seawater (ASW) medium (22). This media is referred to as ASW_m from now on, and its composition is shown in Table 1. ASW_m contained sodium acetate as the sole carbon source (at concentrations specified per experiment), 200mM sodium chloride (instead of 428 mM, as in ASW), ammonium as nitrogen source (instead of nitrate, as in ASW), and five vitamins that were added as supplement. In manganese-supplemented ASW_m, manganese chloride ($MnCl_2$) was added to 200 μM. Cultures were grown at 30 °C in appropriate (100 ml) Erlenmeyer flasks (shaking at 150 rpm) or 96 well polystyrene plates (Corning Inc.) closed with lid and parafilm (shaking at 300 rpm). Plates were incubated in a CLARIOstar plate reader (BMG labtech) and absorbance measurements were done at 600 nm (A_{600}) and with path length-correction, so to present absorbance per 1 cm.

Electron microscopy (EM) and Energy Dispersive X-ray spectroscopy (EDS) analysis of AzwK-3b cultures. A culture of AzwK-3b (40 ml in 100 ml Erlenmeyer flasks) was inoculated in ASW_m without manganese and nitrite, and containing 50 mM acetate. After 3 days at 150 rpm and 30 °C (by which time the culture reached the stationary phase), dilutions (25x – 200x) were made for a second passage of culture in the same medium, supplemented with 200 μM manganese. After further 2 days of culturing, samples for EM were prepared as follows: Cells from 2.5 ml culture were harvested by centrifugation (5 min at 5,000 g), and the supernatant was discarded. From here, several washing and dehydration steps were conducted by re-suspending the pellet in different solutions and subsequently centrifuging for 5 min at 5,000 g (supernatant discarded): (1) first, pellets were twice re-suspended in ASW_m medium basis (no manganese, no acetate, no ammonium, no nitrite, no trace metals); (2) afterwards, samples were re-suspended in 200 μl 70 % ethanol, incubated for 1 min, and pelleted by centrifugation; (3) for a washing-dehydration step, pellets were twice re-suspended in 200 μl 100 % ethanol and harvested by centrifugation; (4) finally, samples were re-suspended in 100 μl of 100 % ethanol. This suspension was then applied to Transmission Electron Microscopy (TEM) grids (Lacey carbon film coated copper grids (Agar Scientific)) by pipetting, in 1 μl portions (allowed to dry in between), until a total of 2 or 5 μl was accumulated (on different grids).

377 EM analysis was done on a Gemini SEM 500 (Zeiss) equipped with EDS X-Max detector
378 (Oxford Instruments). Data analysis was done on the associated AZtec software, which
379 contained the spectral information to identify individual elements. Electron micrographs had
380 the best quality in scanning transmission EM mode (STEM) with a high angle annular dark
381 field detector (HAADF). For EDS, the sample needed to be moved, and the HAADF detector
382 had to be withdrawn, so the location of analysis after changing the setup was confirmed by
383 additional scanning EM (SEM) recording.

384

385 **Large inocula preparation for nitrite-assays.** AzwK-3b was grown in Erlenmeyer flasks
386 (usually 40 ml culture volume in 100 ml Erlenmeyer flasks) in ASW_m with 25 mM acetate. The
387 culture absorbance A_{600} was recorded regularly on a Spectronic 200 spectrophotometer
388 (Thermo Fisher) with 1 cm path length polystyrene cuvettes, and inocula were sampled at
389 various stages of the growth curve (e.g. see Figures S4, S5, S8). This culture was used to
390 inoculate into 96 well plates, which were supplemented by 1:1 dilution with fresh medium
391 supplemented with manganese and/or nitrite and other additives, as described for the
392 particular results shown (see legends of Figures 3, 7, S6, S8). Where noted (see respective
393 figure captions), the fresh medium used for dilution was also supplemented with NADH or
394 hydrogen peroxide at different concentrations. NADH or hydrogen peroxide were added as
395 last additives (to prevent reaction e.g. between hydrogen peroxide and Mn^{II} before
396 inoculation) and the completed fresh medium was used immediately.

397

398 **Growth curve fitting and analysis.** Growth curves were analyzed using the R-package Grofit
399 (23) applying the Gompertz growth model (23, 24). Plate reader data (measurements every
400 10 minutes) were de-noised by averaging over 6 measurements (i.e. hourly averages). The
401 maximum A_{600} reached was read directly from the data. For curve fitting, all data later than
402 the maximum A_{600}, i.e. decaying growth phase, were removed. Then, the data was read
403 backwards in time to find the first reading that was below 5 % of the maximum A_{600}. This data-
404 trimming was done to facilitate the fitting of the Gompertz growth model without bias from
405 different lag-phases (which were ignored), or different lengths and scales of decaying phases

406 recorded. From the resulting model, the maximum growth rate μ (in $A_{600\ nm}$(a.u.) per hour)
407 was recorded.

408

409 **Preparation of cell-free bio-manganese oxide.** The procedure was adapted from previous
410 publications using the cell free supernatant of *Roseobacter sp.* AzwK-3b grown in complex
411 medium (16–19). AzwK-3b was grown in ASW_m supplemented with 50 mM sodium acetate
412 for nine days, using individual 50 or 100 ml cultures in 100 or 200 ml Erlenmeyer flasks,
413 respectively, at 30 °C with shaking (150 rpm). In total, 2 liters of culture was prepared, cells
414 were removed by centrifugation (5 minutes at 10,000 g) and the supernatants were
415 combined. From this (cell-free) supernatant, individual samples of 100 or 200 ml were
416 prepared and supplemented with 200 μM manganese chloride, $MnCl_2$. Manganese oxidation
417 was allowed to proceed for five days at 30 °C with shaking (150 rpm), after which the
418 manganese oxide was harvested by centrifugation (5 minutes at 10,000 g) from each 50/100
419 ml sample . These were combined and washed by suspending in 25 ml acetate-free ASW_m
420 medium and re-sedimented by centrifugation. The pellet was brown in appearance and had
421 considerable volume, indicating co-precipitation of organic material (e.g. secreted proteins)
422 from the cell-culture supernatant. To estimate the amount of manganese precipitated in the
423 assay, the supernatants from centrifugation and the washing steps were combined, and the
424 residual manganese determined by the 3,3',5,5'-tetramethylbenzidine (TMB)-assay (25) for
425 soluble manganese. Note that this was not a precise quantification, but was conclusive
426 enough to allow conservative stoichiometric relations to be inferred. In particular, we inferred
427 that ca. 75 % of the 200 μM manganese chloride had been removed from the solution and
428 this value was used for downstream calculations. The MnO_x precipitate was suspended in an
429 appropriate volume of the acetate-free medium to produce a "10 mM" suspension of
430 manganese oxide, and this value is used in the manuscript as indicator for manganese oxide
431 concentration. The pH was 8.2, which is well in line with the pH 8.0 of the ASW_m medium,
432 showing that the suspended manganese oxide did not alter the pH.

433

434 **Quantification of nitrite, nitrate and acetate.** Quantification was done by Ion
435 Chromatography (IC) on a DIONEX ICS-5000+ (ThermoFisher, UK) equipped with conductivity

436 detector and a DIONEX IonPac AS11-HC-4µm (2 x 250 mm ThermoFisher, UK) anion
437 separation column with appropriate guard column. Separation was achieved with a
438 potassium hydroxide (KOH) gradient, with the KOH added to the eluent by electrolytic eluent
439 generation and, before conductivity detection, removed by electrochemical eluent
440 suppression (both the generation and suppression units are part of the ICS-5000+ system).
441 Culture samples were filtered (0.22 µm polyamide spin filter Costar Spin-X, Corning, NY/USA)
442 and 10-fold diluted with MilliQ-water (checked for purity by measuring resistance (R); R > 18.2
443 MΩ), of which 2.5 µl were injected for IC separation. The IC was run at flow rate of 0.38
444 ml/min, column temperature 30 °C, and a conductivity detector cell temperature of 35 °C.
445 The gradient condition, for the 37 minutes total run-time including 7 minutes pre-
446 equilibration time, was: 7 minutes pre-run (equilibration) at 1.5 mM KOH before injection;
447 remain 8 minutes at 1.5 mM KOH; increase to 15 mM KOH over 10 minutes; increase to 24
448 mM KOH over 5 minutes; increase to 60 mM KOH over 1 minutes; remain at 60 mM KOH over
449 6 minutes. Reference samples with known concentrations were run for calibration, from
450 which the concentrations of nitrite, nitrate, and acetate in the samples was inferred. During
451 the course of the experiments (see below) evaporation of the samples was noted (indicated
452 by the increase in the peak area of chloride, which is expected to be unaltered by any biologic
453 means and therefore should have displayed no concentration change). To correct for this
454 evaporation effect, the concentrations of the analytes of interest were corrected by the same
455 ratio as that obtained from the chloride peak area (from the beginning and end point samples
456 of a particular time-course experiment).

457 ## Author Contributions

458 CZ, JCO and OSS designed the study and the experiments. CZ performed the
459 experiments and analyzed the data. All authors contributed to the writing of the manuscript
460 and have given approval to the final version.

461 ## Acknowledgments

462 This work is funded by The University of Warwick and by the Biotechnological and Biological,
463 Natural Environment, and Engineering and Physical Sciences Research Councils (BB–, NE-,
464 and EPSRC), with grant IDs: BB/K003240/2 (to OSS), NE/K009044/1 (to JCO) and

BB/M017982/1 (to the Warwick Integrative Synthetic Biology Centre, WISB). We would like to thank Colleen Hansel (Woods Hole Oceanographic Institution) for providing *Roseobacter sp.* AzwK-3b, and Steve York from the Electron Microscopy research technology platform (EM RTP) at the Materials Science Department (Physics, University of Warwick) for EM/EDS measurements.

References

1. Lowenstam H (1981) Minerals formed by organisms. *Science* 211(4487):1126–1131.

2. Hansel CM (2017) Manganese in marine microbiology. *Advances in Microbial Physiology - Microbiology of Metal Ions*, ed Poole RK (Academic Press, Oxford), pp 37–83.

3. Nealson KH (2006) The manganese-oxidizing bacteria. *Prokaryotes* 5:222–231.

4. Ghiorse WC (1984) Biology of iron-and manganese-depositing bacteria. *Annu Rev Microbiol* 38(1):515–550.

5. Spiro TG, Bargar JR, Sposito G, Tebo BM (2010) Bacteriogenic manganese oxides. *Acc Chem Res* 43(1):2–9.

6. Blöthe M, Wegorzewski A, Müller C, Simon F, Kuhn T, Schippers A (2015) Manganese-cycling microbial communities inside deep-sea manganese nodules. *Environ Sci Technol* 49(13):7692–7700.

7. Tebo BM, Johnson HA, McCarthy JK, Templeton AS (2005) Geomicrobiology of manganese(II) oxidation. *Trends Microbiol* 13(9):421–428.

8. Geszvain K, Butterfield C, Davis RE, Madison AS, Lee S-W, Parker DL, Soldatova A, Spiro TG, Luther GW, Tebo BM (2012) The molecular biogeochemistry of manganese(II) oxidation. *Biochem Soc Trans* 40(6):1244–1248.

9. Myers CR, Nealson KH (1988) Bacterial manganese reduction and growth with manganese oxide as the sole electron acceptor. *Science* 240(4857):1319–21.

10. Venkateswaran K, Moser DP, Dollhopf ME, Lies DP, Saffarini DA, MacGregor BJ, Ringelberg DB, White DC, Nishijima M, Sano H, Burghardt J, Stackebrandt E, Nealson KH (1999) Polyphasic taxonomy of the genus *Shewanella* and description of *Shewanella*

493 *oneidensis sp. nov. Int J Syst Bacteriol* 49(2):705–24.

494 11. Lovley DR (1993) Dissimilatory metal reduction. *Annu Rev Microbiol* 47:263–90.

495 12. Emerson D, Fleming EJ, McBeth JM (2010) Iron-oxidizing bacteria: an environmental
496 and genomic perspective. *Annu Rev Microbiol* 64:561–83.

497 13. Remucal CK, Ginder-Vogel M (2014) A critical review of the reactivity of manganese
498 oxides with organic contaminants. *Environ Sci Process Impacts* 16(6):1247–66.

499 14. Sunda WG, Kieber DJ (1994) Oxidation of humic substances by manganese oxides yields
500 low-molecular-weight organic substrates. *Nature* 367(6458):62–64.

501 15. Keiluweit M, Nico P, Harmon ME, Mao J, Pett-Ridge J, Kleber M (2015) Long-term litter
502 decomposition controlled by manganese redox cycling. *Proc Natl Acad Sci*
503 112(38):E5253–E5260.

504 16. Hansel CM, Francis CA (2006) Coupled photochemical and enzymatic Mn(II) oxidation
505 pathways of a planktonic *Roseobacter*-Like bacterium. *Appl Environ Microbiol*
506 72(5):3543–9.

507 17. Andeer PF, Learman DR, McIlvin M, Dunn JA, Hansel CM (2015) Extracellular haem
508 peroxidases mediate Mn(II) oxidation in a marine *Roseobacter* bacterium via
509 superoxide production. *Environ Microbiol* 17(10):3925–3936.

510 18. Learman DR, Voelker BM, Vazquez-Rodriguez AI, Hansel CM (2011) Formation of
511 manganese oxides by bacterially generated superoxide. *Nat Geosci* 4(2):95–98.

512 19. Learman DR, Voelker BM, Madden AS, Hansel CM (2013) Constraints on superoxide
513 mediated formation of manganese oxides. *Front Microbiol* 4:262.

514 20. Learman DR, Wankel SD, Webb SM, Martinez N, Madden AS, Hansel CM (2011)
515 Coupled biotic–abiotic Mn(II) oxidation pathway mediates the formation and structural
516 evolution of biogenic Mn oxides. *Geochim Cosmochim Acta* 75(20):6048–6063.

517 21. Luther GW (2010) The role of one- and two-electron transfer reactions in forming
518 thermodynamically unstable intermediates as barriers in multi-electron redox
519 reactions. *Aquat Geochemistry* 16(3):395–420.

520 22. Wilson WH, Carr NG, Mann NH (1996) The effect of phosphate status on the kinetics

of cyanophage infection in the oceanic cyanobacterium *Synechococcus sp.* WH78031. *J Phycol* 32(4):506–516.

23. Kahm M, Hasenbrink G, Lichtenberg-Fraté H, Ludwig J, Kschischo M (2010) Grofit: fitting biological growth curves with R. *J Stat Softw* 33(7):1–21.

24. Zwietering MH, Jongenburger I, Rombouts FM, van 't Riet K (1990) Modeling of the bacterial growth curve. *Appl Environ Microbiol* 56(6):1875–81.

25. Bosch Serrat F (1998) 3,3',5,5'-Tetramethylbenzidine for the colorimetric determination of manganese in water. *Mikrochim Acta* 129(1–2):77–80.

26. Tebo BM, Bargar JR, Clement BG, Dick GJ, Murray KJ, Parker D, Verity R, Webb SM (2004) Biogenic manganese oxides: properties and mechanisms of formation. *Annu Rev Earth Planet Sci* 32(1):287–328.

27. Templeton AS, Staudigel H, Tebo BM (2005) Diverse Mn(II)-oxidizing bacteria isolated from submarine basalts at Loihi seamount. *Geomicrobiol J* 22(3–4):127–139.

28. Francis CA, Co E-M, Tebo BM (2001) Enzymatic manganese(II) oxidation by a marine α-proteobacterium. *Appl Environ Microbiol* 67(9):4024–4029.

29. Johnson HA, Tebo BM (2008) In vitro studies indicate a quinone is involved in bacterial Mn(II) oxidation. *Arch Microbiol* 189(1):59–69.

30. Wang X, Wiens M, Divekar M, Grebenjuk VA, Schröder HC, Batel R, Müller WEG (2010) Isolation and characterization of a Mn(II)-oxidizing *Bacillus* strain from the demosponge *Suberites domuncula*. *Mar Drugs* 9(1):1–28.

31. Kraft B, Strous M, Tegetmeyer HE (2011) Microbial nitrate respiration – Genes, enzymes and environmental distribution. *J Biotechnol* 155(1):104–117.

32. Cavaliere M, Feng S, Soyer OS, Jiménez JI (2017) Cooperation in microbial communities and their biotechnological applications. *Environ Microbiol* 19(8):2949–2963.

33. Allen B, Gore J, Nowak MA (2013) Spatial dilemmas of diffusible public goods. *Elife* 2:e01169.

34. West SA, Diggle SP, Buckling A, Gardner A, Griffin AS (2007) The social lives of microbes. *Annu Rev Ecol Evol Syst* 38(1):53–77.

549 35. Allison SD (2005) Cheaters, diffusion and nutrients constrain decomposition by
550 microbial enzymes in spatially structured environments. *Ecol Lett* 8(6):626–635.

551 36. Keim CN, Nalini HA, de Lena JC (2015) Manganese oxide biominerals from freshwater
552 environments in Quadrilatero Ferrifero, Minas Gerais, Brazil. *Geomicrobiol J* 32(6):549–
553 559.

554 37. Cammack R, Joannou C., Cui X-Y, Torres Martinez C, Maraj SR, Hughes MN (1999)
555 Nitrite and nitrosyl compounds in food preservation. *Biochim Biophys Acta - Bioenerg*
556 1411(2–3):475–488.

557 38. Müller-Herbst S, Mühlig A, Kabisch J, Rohtraud Pichner, Scherer S (2015) The food
558 additives nitrite and nitrate and microbiological safety of food products. *Am J Microbiol*
559 6(1):1–3.

560 39. Zhou Y, Oehmen A, Lim M, Vadivelu V, Ng WJ (2011) The role of nitrite and free nitrous
561 acid (FNA) in wastewater treatment plants. *Water Res* 45(15):4672–82.

562 40. Robinson KM, Beckman JS (2005) Synthesis of peroxynitrite from nitrite and hydrogen
563 peroxide. *Methods Enzymol*:207–214.

564 41. Heaselgrave W, Andrew PW, Kilvington S (2010) Acidified nitrite enhances hydrogen
565 peroxide disinfection of acanthamoeba, bacteria and fungi. *J Antimicrob Chemother*
566 65(6):1207–14.

567 42. Kono Y, Shibata H, Adachi K, Tanaka K (1994) Lactate-dependent killing of *Escherichia*
568 *coli* by nitrite plus hydrogen peroxide: a possible role of nitrogen dioxide. *Arch Biochem*
569 *Biophys* 311(1):153–159.

570 43. Luther, III GW, Popp JI (2002) Kinetics of the abiotic reduction of polymeric manganese
571 dioxide by nitrite: an anaerobic nitrification reaction. *Aquat Geochemistry* 8(1):15–36.

572 44. Martínez MC, Andriantsitohaina R (2009) Reactive nitrogen species: molecular
573 mechanisms and potential significance in health and disease. *Antioxid Redox Signal*
574 11(3):669–702.

575 45. Tharmalingam S, Alhasawi A, Appanna VP, Lemire J, Appanna VD (2017) Reactive
576 nitrogen species (RNS)-resistant microbes: adaptation and medical implications. *Biol*
577 *Chem* 398(11):1193–1208.

578 46. Watts RJ, Sarasa J, Loge FJ, Teel AL (2005) Oxidative and reductive pathways in
579 manganese-catalyzed Fenton's reactions. *J Environ Eng* 131(1):158–164.

580 47. Jiang S, Ashton WR, Tseung ACC (1991) An observation of homogeneous and
581 heterogeneous catalysis processes in the decomposition of H_2O_2 over MnO_2 and
582 $Mn(OH)_2$. *J Catal* 131(1):88–93.

583 48. Kanungo SB, Parida KM, Sant BR (1981) Studies on MnO_2—III. The kinetics and the
584 mechanism for the catalytic decomposition of H_2O_2 over different crystalline
585 modifications of MnO_2. *Electrochim Acta* 26(8):1157–1167.

586 49. Rophael MW, Petro NS, Khalil LB (1988) II — kinetics of the catalytic decomposition of
587 hydrogen peroxide solution by manganese dioxide samples. *J Power Sources*
588 22(2):149–161.

589 50. Do S-H, Batchelor B, Lee H-K, Kong S-H (2009) Hydrogen peroxide decomposition on
590 manganese oxide (pyrolusite): Kinetics, intermediates, and mechanism. *Chemosphere*
591 75(1):8–12.

592 51. Li W, Liu Z, Liu C, Guan Y, Ren J, Qu X (2017) Manganese dioxide nanozymes as
593 responsive cytoprotective shells for individual living cell encapsulation. *Angew Chem*
594 *Int Ed Engl* 56(44):13661–13665.

595 52. Broughton DB, Wentworth RL (1947) Mechanism of decomposition of hydrogen
596 peroxide solutions with manganese dioxide. I. *J Am Chem Soc* 69(4):741–744.

597 53. Broughton DB, Wentworth RL, Laing ME (1947) Mechanism of decomposition of
598 hydrogen peroxide solutions with manganese dioxide. II. *J Am Chem Soc* 69(4):744–
599 747.

600 54. Seaver LC, Imlay JA (2001) Alkyl hydroperoxide reductase is the primary scavenger of
601 endogenous hydrogen peroxide in *Escherichia coli*. *J Bacteriol* 183(24):7173–7181.

602 55. Farr SB, Kogoma T (1991) Oxidative stress responses in *Escherichia coli* and *Salmonella*
603 *typhimurium*. *Microbiol Rev* 55(4):561–85.

604 56. Nathan C, Bryk R, Griffin P (2000) Peroxynitrite reductase activity of bacterial
605 peroxiredoxins. *Nature* 407(6801):211–215.

606 57. Zamocky M, Furtmüller PG, Obinger C (2008) Evolution of catalases from bacteria to

607 humans. *Antioxid Redox Signal* 10(9):1527–1548.

608 58. Mishra S, Imlay J (2012) Why do bacteria use so many enzymes to scavenge hydrogen
609 peroxide? *Arch Biochem Biophys* 525(2):145–60.

610 59. Diaz JM, Hansel CM, Voelker BM, Mendes CM, Andeer PF, Zhang T (2013) Widespread
611 production of extracellular superoxide by heterotrophic bacteria. *Science*
612 340(6137):1223–6.

613 60. Camargo JA, Alonso A (2006) Ecological and toxicological effects of inorganic nitrogen
614 pollution in aquatic ecosystems: A global assessment. *Environ Int* 32(6):831–49.

615 61. Cleemput O, Samater AH (1995) Nitrite in soils: accumulation and role in the formation
616 of gaseous N compounds. *Fertil Res* 45(1):81–89.

617 62. Riley WJ, Ortiz-Monasterio I, Matson PA (2001) Nitrogen leaching and soil nitrate,
618 nitrite, and ammonium levels under irrigated wheat in Northern Mexico. *Nutr Cycl*
619 *Agroecosystems* 61(3):223–236.

620 63. Lawniczak AE, Zbierska J, Nowak B, Achtenberg K, Grześkowiak A, Kanas K (2016)
621 Impact of agriculture and land use on nitrate contamination in groundwater and
622 running waters in central-west Poland. *Environ Monit Assess* 188(3):172.

623 64. Beeckman F, Motte H, Beeckman T (2018) Nitrification in agricultural soils: impact,
624 actors and mitigation. *Curr Opin Biotechnol* 50:166–173.

625 65. Cruz-García C, Murray AE, Klappenbach JA, Stewart V, Tiedje JM (2007) Respiratory
626 nitrate ammonification by *Shewanella oneidensis* MR-1. *J Bacteriol* 189(2):656–662.

627 66. Chen Y, Wang F (2015) Insights on nitrate respiration by *Shewanella*. *Front Mar Sci* 1:80.

628 67. Zhang H, Fu H, Wang J, Sun L, Jiang Y, Zhang L, Gao H (2013) Impacts of Nitrate and
629 Nitrite on Physiology of *Shewanella oneidensis*. *PLoS One* 8(4):e62629.

630 68. Quijano C, Trujillo M, Castro L, Trostchansky A (2016) Interplay between oxidant
631 species and energy metabolism. *Redox Biol* 8:28–42.

632 69. Davies KJ (1995) Oxidative stress: the paradox of aerobic life. *Biochem Soc Symp* 61:1–
633 31.

634 70. Gutteridge JM (1994) Biological origin of free radicals, and mechanisms of antioxidant

635 protection. *Chem Biol Interact* 91(2–3):133–40.

636 71. Korshunov S, Imlay JA (2010) Two sources of endogenous hydrogen peroxide in
637 *Escherichia coli*. *Mol Microbiol* 75(6):1389–1401.

638 72. van der Heijden J, Vogt SL, Reynolds LA, Peña-Díaz J, Tupin A, Aussel L, Finlay BB (2016)
639 Analysis of bacterial survival after exposure to reactive oxygen species or antibiotics.
640 *Data Br* 7:894–899.

641 73. van der Heijden J, Vogt SL, Reynolds LA, Peña-Díaz J, Tupin A, Aussel L, Finlay BB (2016)
642 Exploring the redox balance inside gram-negative bacteria with redox-sensitive GFP.
643 *Free Radic Biol Med* 91:34–44.

644 74. Seaver LC, Imlay JA (2001) Hydrogen peroxide fluxes and compartmentalization inside
645 growing *Escherichia coli*. *J Bacteriol* 183(24):7182–7189.

646 75. González-Flecha B, Demple B (1995) Metabolic sources of hydrogen peroxide in
647 aerobically growing *Escherichia coli*. *J Biol Chem* 270(23):13681–13687.

648 76. Christie-Oleza JA, Scanlan DJ, Armengaud J (2015) “You produce while I clean up”, a
649 strategy revealed by exoproteomics during *Synechococcus* - *Roseobacter* interactions.
650 *Proteomics* 15(20):3454–3462.

651 77. Gore J, Youk H, van Oudenaarden A (2009) Snowdrift game dynamics and facultative
652 cheating in yeast. *Nature* 459(7244):253–6.

653 78. Kümmerli R, Jiricny N, Clarke LS, West SA, Griffin AS (2009) Phenotypic plasticity of a
654 cooperative behaviour in bacteria. *J Evol Biol* 22(3):589–98.

655 79. Francis CA, Tebo BM (2002) Enzymatic manganese(II) oxidation by metabolically
656 dormant spores of diverse *Bacillus* species. *Appl Environ Microbiol* 68(2):874–880.

657 80. Bargar J., Tebo B., Villinski J. (2000) In situ characterization of Mn(II) oxidation by spores
658 of the marine *Bacillus sp.* strain SG-1. *Geochim Cosmochim Acta* 64(16):2775–2778.

659 81. Tang YJ, Laidlaw D, Gani K, Keasling JD (2006) Evaluation of the effects of various
660 culture conditions on Cr(VI) reduction by *Shewanella oneidensis* MR-1 in a novel high-
661 throughput mini-bioreactor. *Biotechnol Bioeng* 95(1):176–184.

662 82. Balch WE, Fox GE, Magrum LJ, Woese CR, Wolfe RS (1979) Methanogens: reevaluation

663 of a unique biological group. *Microbiol Rev* 43(2):260–96.

664

665

Figures

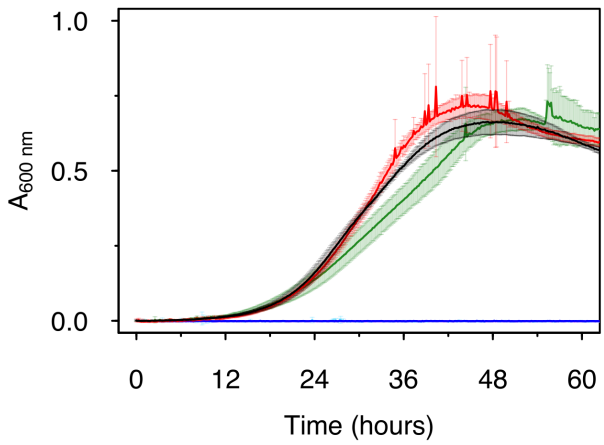

Figure 1. Effect of Mn^{II} on the growth of *Roseobacter sp.* AzwK-3b in the defined growth medium (see Table 1). The concentrations of manganese were 0 μM (black), 200 μM (red) and 500 μM (dark green), with no growth (zero line) in the respective non-inoculated controls (blue, magenta, light blue). Cultures were grown in a 96 well plate (200 μl culture) with shaking and absorbance measurement every 10 minutes (see *Methods*).

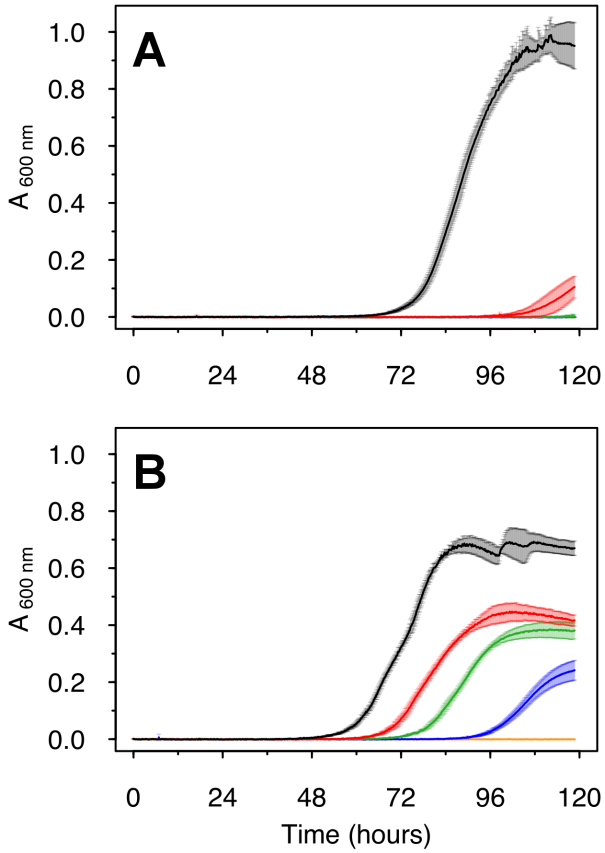

674

675 **Figure 2.** Growth of *Roseobacter sp.* AzwK-3b in the defined growth medium supplemented
676 with sodium nitrite. Media were prepared without (Figure A) or with (Figure B) 200 μM
677 manganese chloride, $Mn^{II}Cl_2$. Nitrite-concentrations were 0 mM (black), 0.25 mM (red), 0.5
678 mM (green), 1 mM (dark blue) and 2.5 mM (light blue). All conditions were tested in
679 triplicates, and the growth curves represent averages and their standard deviations (see
680 *Methods*).

681

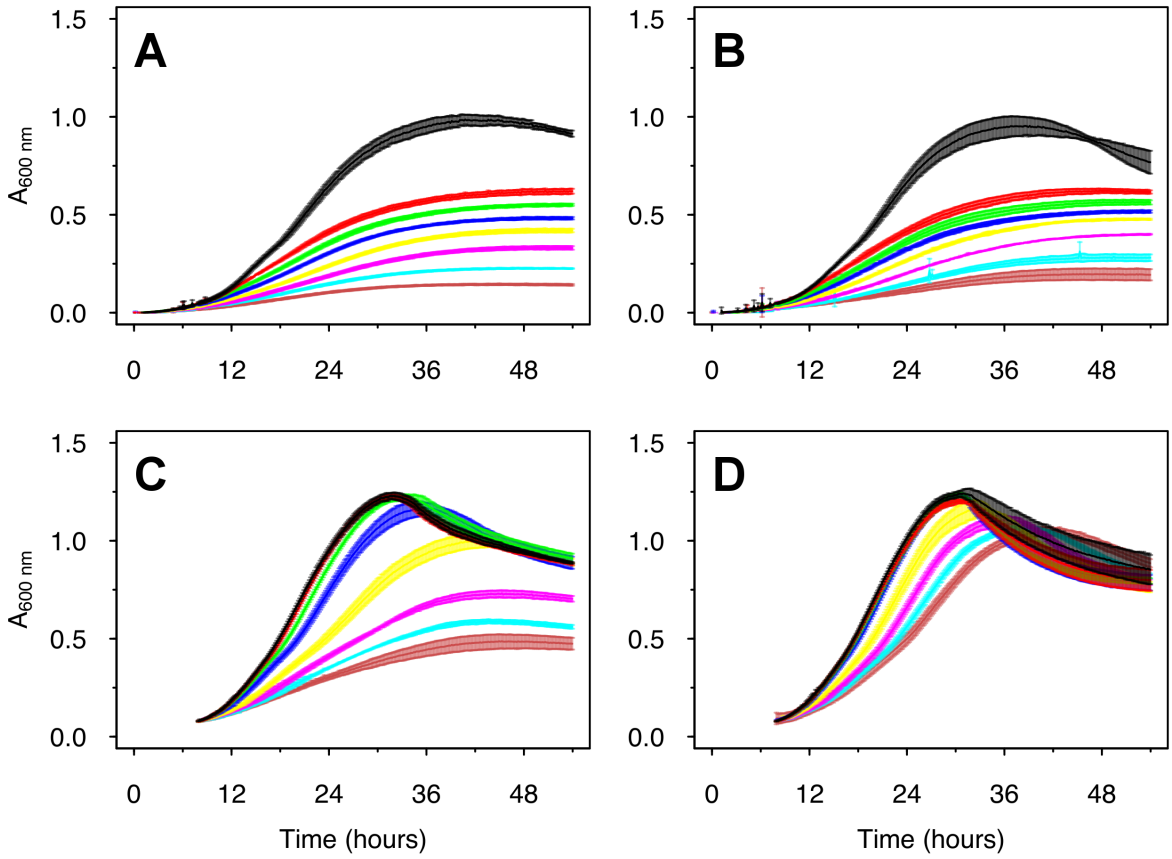

682

683 **Figure 3.** Larger AzwK-3b inocula are less inhibited by nitrite. A pre-culture without
684 manganese or nitrite was grown and sampled in the exponential growth phase (Figure S4) to
685 prepare inocula from a very early time point in the exponential phase (IT 1, Figures A and B),
686 and from a later time point (IT 2, Figures C and D; both sampled in first third of exponential
687 phase). These inocula were 1:1 diluted with fresh medium, and tested for growth at different
688 nitrite concentrations (see below for colour code) without (A, C) or with (B, D) 200 μM $Mn^{II}Cl_2$
689 supplement. The nitrite concentrations were: Black – control no nitrite. Red – 0.25 mM nitrite.
690 Green – 0.5 mM nitrite. Blue – 1 mM nitrite. Yellow – 2 mM nitrite. Magenta – 5 mM nitrite.
691 Light blue – 7.5 mM nitrite. Dark red – 10 mM nitrite. Growth curves show the averages and
692 standard deviations over a triplicate analysis (see *Methods*).

693

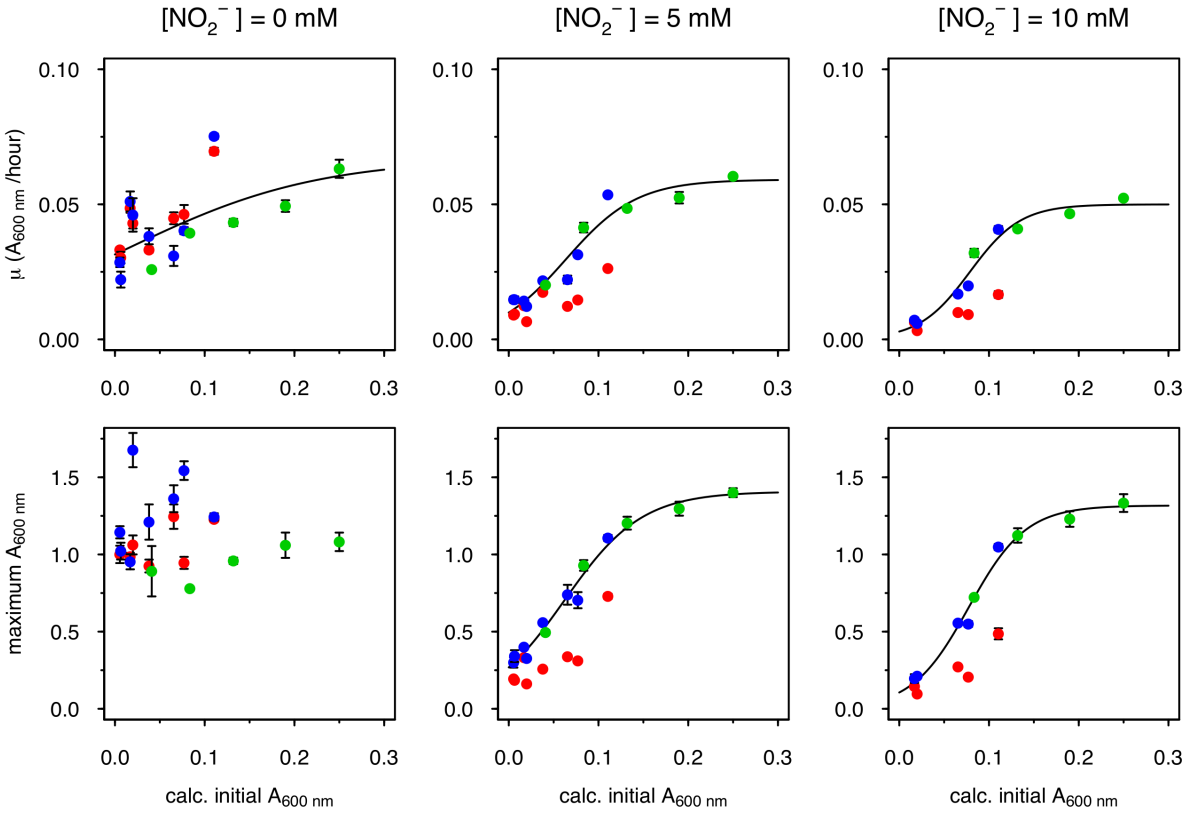

694

695 **Figure 4.** Inoculum-size effect on MnO_X mediated mitigation of nitrite-inhibition. Data from
696 different AzwK-3b growth experiments of similar type ("Large inocula", see *Methods*) were
697 analyzed for the maximum A_{600} and growth rate by fitting the growth curves. Nitrite-
698 concentrations of the main-cultures are indicated as headings of the figure-rows. The x-axes
699 show the calculated A_{600} of the cultures after diluting them 1:1 for the main-culture, while
700 the y-axes show the maximum A_{600} and maximum growth rate as calculated with the
701 Gompertz model (23, 24)) (see *Methods*). The colours represent different conditions: **Red:**
702 Neither pre-, nor main-culture contained manganese; **Blue:** Pre-culture without, main-culture
703 with manganese; **Green:** both pre- and main-culture with manganese. The black curve is a
704 sigmoidal fit (logistic model) from the Grofit R-package (23), for the results of the combined
705 blue and green dataset where the nitrite-exposed main-cultures all contained manganese.

706

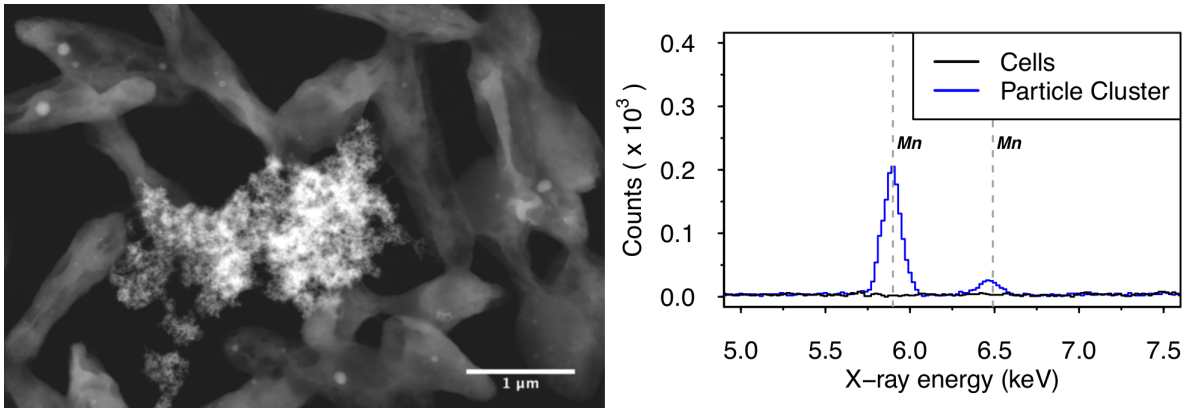

Figure 5. Scanning transmission electron micrograph (left figure, high angle annular dark field) of (granular) manganese-containing precipitate (center) surrounded by AzwK-3b cells, and associated energy dispersive X-ray spectroscopic analysis (right figure) in this location. Only the energy range containing the manganese-specific X-ray energies at 5.90 keV (K_{α}^{I}) and 6.49 keV (K_{β}^{I}) is shown, and the manganese transitions are indicated by vertical gray dashed lines.

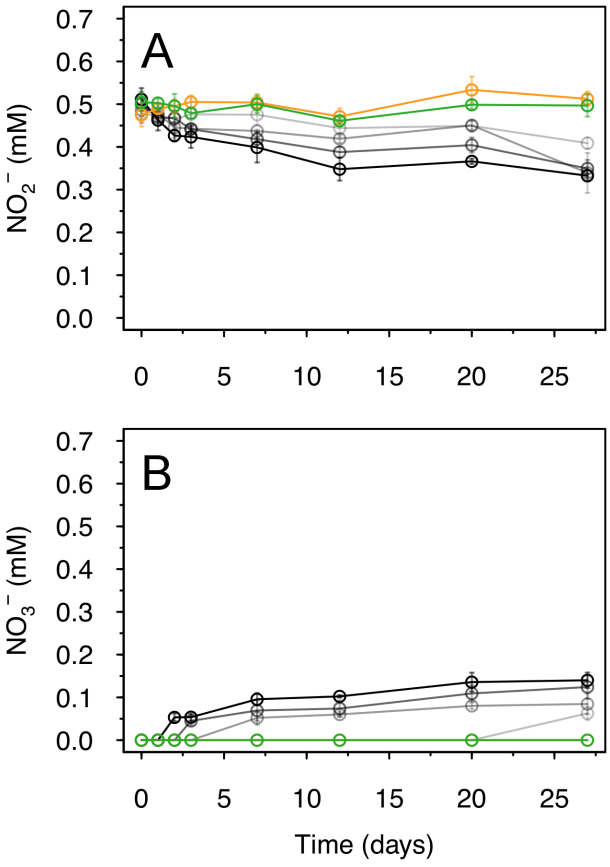

Figure 6. Oxidation of nitrite by biogenic manganese oxide (MnO_X) produced in cell-free culture supernatant of AzwK-3b. The figures show the concentration of nitrite (A) and nitrate

(B), determined by ion chromatography, over time (note that concentrations were corrected for the IC-peak from chloride, to account for evaporation during the experiment). As controls, samples without MnO_X (green), or with MnO_2 powder (orange) were included in the experiment (see *Methods*). The samples with AzwK-3b cell-free manganese oxide contained (from grey to black) 0.2, 0.5, 1 and 2 mM manganese oxide equivalent (see *Methods*).

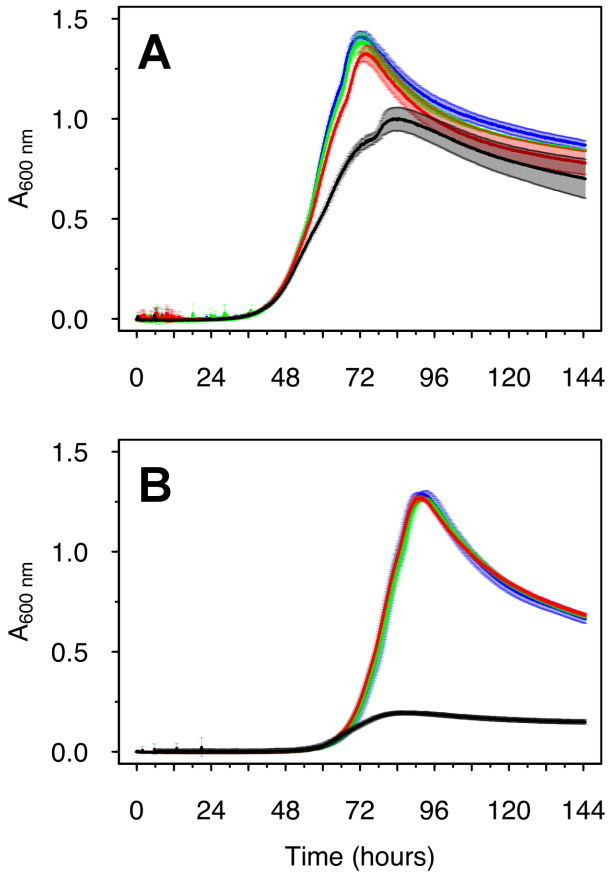

Figure 7. Reductive power (NADH) mitigates the growth inhibitory effects of nitrite in AzwK-3b. Cultures (pre- and main-culture without manganese) were grown in the absence (A) and presence (B) of 5 mM nitrite and supplement of 0, 50, 100 and 200 μM NADH (black, red, green and blue) at the start of the culture.

Tables

Base salts (1 x AzwK-3b medium)	
Sodium chloride (NaCl)	200 mM
Ammonium chloride (NH_4Cl)	8.82 mM
Potassium chloride (KCl)	6.71 mM
di-potassium hydrogenphosphate (KH_2PO_4)	131 µM
Magnesium sulphate ($MgSO_4$)	14.2 mM
Magnesium chloride ($MgCl_2$)	9.84 mM
Calcium chloride ($CaCl_2$)	3 mM
Tris(hydroxymethyl)aminomethane (TRIS)	1.1 mM
pH of the medium	**8.0**
Trace metal solutio (1,000 x)	
Copper chloride ($CuCl_2$)	32 µM
Zink sulphate ($ZnSO_4$)	765 µM
Cobalt chloride ($CoCl_2$)	169 µM
Sodium molybdate (Na_2MoO_4)	1.65 mM
Boric acid (H_3BO_3)	46.3 mM
Nickel chloride ($NiCl_2$)	4.2 mM
Sodium tungstate (Na_2WoO_4)	243 µM
Sodium selenite (Na_2SeO_3)	228 µM
Additional (1,000 x) supplement solutions	
Iron chloride ($FeCl_3$; prepared in 10 mM HCl, balanced with extra 10 mM NaOH solution)	10.4 mM
Ethylenediaminetetraacetate (EDTA, pH 8.0; sodium salt)	1.34 mM
Manganese chloride ($MnCl_2$, only added where desired)	200 mM
Vitamin supplement (1,000 x)	
Biotin	82 µM
Pyridoxine hydrochloride	484 µM
Thiamine hydrochloride	148 µM
Riboflavin	133 µM
Nicotinic acid	406 µM

Table 1. Detailed composition of the defined AzwK-3b growth medium, ASW_m. The medium was developed starting out from artificial seawater (ASW) (22) with extra trace metals taken from (9, 81) and a 5-vitamin solution identified starting out from Wolfe's vitamin mixture (82).